Long-term surveillance of zinc implant in murine artery: surprisingly steady biocorrosion rate

Adam Drelich[1], **Shan Zhao**[2], **Roger J Guillory II**[1], **Jaroslaw W. Drelich**[2], and **Jeremy Goldman**[1,a]

[1]Department of Biomedical Engineering, Michigan Technological University, Houghton, MI 49931

[2]Department of Material Science and Engineering, Michigan Technological University, Houghton, MI 49931

Abstract

Metallic zinc implanted into the abdominal aorta of rats out to 6 months has been demonstrated to degrade while avoiding responses commonly associated with the restenosis of vascular implants. However, major questions remain regarding whether a zinc implant would ultimately passivate through the production of stable corrosion products or via a cell mediated fibrous encapsulation process that prevents the diffusion of critical reactants and products at the metal surface. Here, we have conducted clinically relevant long term *in vivo* studies in order to characterize late stage zinc implant biocorrosion behavior and products to address these critical questions. We found that zinc wires implanted in the murine artery exhibit steady corrosion without local toxicity for up to at least 20 months post-implantation, despite a steady buildup of passivating corrosion products and intense fibrous encapsulation of the wire. Although fibrous encapsulation was not able to prevent continued implant corrosion, it may be related to the reduced chronic inflammation observed between 10 and 20 months post-implantation. X-ray elemental and infrared spectroscopy analyses confirmed zinc oxide, zinc carbonate, and zinc phosphate as the main components of corrosion products surrounding the Zn implant. These products coincide with stable phases concluded from Pourbaix diagrams of a physiological solution and in vitro electrochemical impedance tests. The results support earlier predictions that zinc stents could become successfully bio-integrated into the arterial environment and safely degrade within a time frame of approximately 1 – 2 years.

Graphical Abstract

[a]Corresponding author: Jeremy Goldman, Ph.D., Associate Professor, Biomedical Engineering Department, Michigan Technological University, Houghton, MI, 49931 USA; Ph: (906) 487-2851; Fax: (906) 487-1717; jgoldman@mtu.edu.
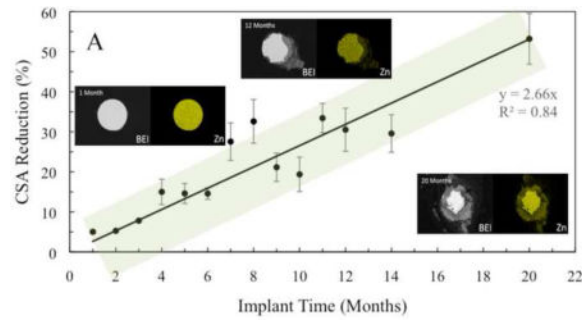
1. Introduction

Coronary stents are an important and beneficial component of assisted vascular remodeling for patients suffering from coronary heart disease [1,2]. Stents are used alongside balloon angioplasty to support the damaged artery and promote revascularization, while lessening the chance of restenosis and other complications. Traditional coronary stents are composed of corrosion-resistant metals such as stainless steel [3]. While these materials meet the mechanical requirements for use in stents they also remain present throughout a patient's lifetime, which can result in complications long after stent deployment. These include chronic inflammation [4], late stage thrombosis [5], and stent strut fracture and damage to local vasculature [6], events that can contribute to restenosis.

In order to mitigate these long-term side effects inherent to current generation coronary stents, a new generation of stents using bioabsorbable material is being developed. Such stents have the potential to match the early benefits of traditional coronary stents while avoiding many of their long-term health risks [7]. Specifically, an ideal bioabsorbable stent would remain mechanically viable in the patient long enough for arterial regeneration to occur, and then be harmlessly broken down and bio-absorbed once its function had been served and before late stage complications could arise [8]. One area of such focus is polymeric stents made of bioabsorbable polymers such as poly L-lactic acid (PLLA). But while polymeric stents have demonstrated acceptable biocompatibility [9], they have significant unavoidable mechanical limitations [10,11] and similar restenosis rates as traditional coronary stents [12].

In recent years attention has increasingly shifted to the development of bioabsorbable metallic stents. In particular, there has been a great deal of focus on magnesium (Mg) [13,14] and iron (Fe) [15,16] and their alloys as candidate materials. While pure Fe stents possess promising mechanical properties and biocompatibility [17], it has also been observed to produce a voluminous oxide layer that repels neighboring tissue and compromises the luminal cross section of the artery in some studies [18], overall potentially falling short of the necessary requirements for a bioabsorbable stent material [19]. Despite additional alloying and processing, Fe corrosion rates are still lower than the benchmark

ideal [17,20,21]. For example, recent long-term studies on biocorrosion of nitride iron scaffolds in rabbit abdominal aorta suggest completion of the degradation process in approximately 4 years [22].

In contrast, Mg has achieved greater success. Both uncoated and coated Mg stents have shown excellent biocompatibility [23], avoiding significant inflammatory responses [24]. Excellent bio-integration is also seen for Mg materials deployed as bone healing assist devices [24,25]. However, it is well known that the base Mg corrodes too quickly *in vivo* for bioabsorbable stent applications, often experiencing extensive material loss even within 1 month [18] and complete degradation as early as 3 months [24]. Mg is also susceptible to corrosion fatigue and mechanical failure [26–28] and generates a rapid buildup of hydrogen gas that can complicate tissue regeneration [29,30]. Alloying has successfully addressed some of these concerns. For instance, Mg-Zr-Sr devices exhibit lower degradation rates [31,32], while MgZnCa glasses have reduced levels of hydrogen gas evolution [33].

Mg based stents have also seen some success in humans. The DREAMS (Drug Eluting Absorbable Magnesium Scaffold) stents from Biotronic have shown promising results in the clinical setting. Clinical trials for both DREAMS 1G [34] and the later DREAMS 2G [35,36] iteration were associated with low thrombosis rates, low incidence of cardiac death and myocardial infarction, and less late lumen loss compared to bare metal and polymer stents, with DREAMS 2G having greater strength, flexibility, and lower neointimal formation than its predecessor. Such trials lasted for up to 12 months. However, early DREAMS designs were also associated with rapid degradation and subsequently high rates of restenosis [37]. DREAMS 2G mitigated this problem with the introduction of a drug-eluting PLLA coating to increase corrosion resistance. However, it is still estimated that ~95% of the magnesium scaffold will be degraded within 12 months, the lower end of the 1 to 2-year ideal degradation benchmark, with a late lumen loss that is higher than comparable stent systems such as ABSORB and DESolve [35,36].

A third candidate material that has emerged in recent years is zinc (Zn) and it's alloys [38]. Zn lacks the critical flaws observed for Mg- and Fe-based alloys, including premature degradation (Mg) and tissue displacement (by iron-oxide corrosion product), and shows promise for coronary stent application [19]. Additionally, pure Zn exhibits a tensile strength of 80–120 MPa, similar to the strength of Mg (86 MPa), but also about three times lower than that of pure Fe (290 MPa) [19]. The elongation to failure of pure Zn (60–80%) is, on the other hand, far superior relative to Mg (13%) and Fe (18%) [19]. Alloying of Zn can improve its strength to the level of Fe and above [39–41], with elongation to failure remaining above values characteristic for pure Mg and Fe [19]. Studies so far on Zn as an experimental stent material have shown good biocompatibility and a rate of degradation between 10–20 μm/yr, which is similar to the 20 μm/yr benchmark value for an ideal bioabsorable material [42,43]. Zn implants were also found to remain intact in the murine arterial wall even after 6 months of residence, with the first 3–6 months after implantation being considered a critical period for coronary stent scaffolding [19]. Finally, Zn is considered relatively nontoxic for humans and an essential trace element. Acute Zn toxicity is associated with symptoms such as abdominal pain, nausea and vomiting, diarrhea, lethargy and light-headedness. Excessive Zn can also cause copper deficiency, resulting in

leukopenia, anemia, and neutropenia [44]. However, moderate symptoms only occur at intake rates of 100–300 mg/day, with acute toxicity at 225–450 mg/day and a median lethal dose (LD50) of 27 g. For the complete degradation of a pure Zn stent, it is estimated that daily intake would be only 150 µg/day [38].

As a novel stent material, no metallographic studies have been conducted to quantify long-term corrosion of Zn implants *in vivo* out to 20 months. It is of utmost importance in an early exploration phase to study the short-term corrosion of a bioabsorbable stent candidate material to confirm its feasibility in a coronary stent setting. Then, once the material has been validated, it is essential to investigate its long-term corrosion behavior as it progresses toward complete break down and tissue clearance. This is especially true for Zn, with earlier studies suggesting possible acceleration in biocorrosion at later time points [38]. To this end, in the present study we report on the corrosion of pure Zn wires implanted in the murine artery wall for up to 20 months. The results reveal consistent and relatively steady corrosion rates for Zn. This was unexpected due to the formation of passivating corrosion products and fibrous encapsulation of the wire, each of which would be expected to retard continued zinc corrosive activity.

2. Experimental

2.1 In vivo implantation and sample preparation

Zn wire from Goodfellow (99.99+% purity) with a diameter of 0.25 mm was used in this study. The wire was cut into 2 cm - long segments and sanitized in 70% ethanol before being surgically implanted into live Sprague-Dawley rat arteries. Each wire was implanted into the wall of the abdominal aorta of a rat following the surgical protocol reported previously [18]. Briefly, the adventitial layer of the abdominal aorta was penetrated by the wire, which was then advanced into or near the arterial media for the entire length of the specimen. The animal study was approved by the Michigan Technological University Institutional Animal Care and Use Committee (IACUC) and was performed in accordance with the Panel on Euthanasia of the American Veterinary Medical Association.

At specified end points, rats were euthanized and arteries containing the degraded wires removed every month for 12 months, along with two additional samples at 14 and 20 months. Approximately half of each implanted wire was used for histological analysis (briefly presented in this publication and more thoroughly characterized in a recent publication [45]), while the remaining half was used for imaging and metallographic analysis.

Wire segments used for metallographic analysis were received still embedded within the rat artery, although an effort was made to trim the surrounding tissue. Samples were stored in absolute ethanol at room temperature for several days and then placed in a dessicator until the remaining biological material dried. Each wire sample was affixed to a plastic mounting clip, placed in a section of 2/5"-diameter plastic tubing, and embedded in ultra-thin epoxy resin. Once cured the plastic tubing was then removed to create an epoxy tube containing the sample. A razor blade affixed to a micrometer was then used to cross-section the samples into slices 0.5–1 mm thick.

Cross-sections from each wire were then super glued onto a polystyrene disc and affixed to the bottom of a cylindrical plastic mold, before once more being embedded in ultra-thin epoxy resin. Once cured the samples were submerged briefly in acetone to remove the remaining polystyrene and super glue to expose the surfaces of the cross-sections on each epoxy mount. All samples were then polished first by hand using P1500 silicon carbide paper with blue lube followed by a spin polish on a 1 μm diamond NAPPAD with red lube.

2.2 Sample imaging and analysis

All samples were carbon coated prior to Scanning Electron Microscope (SEM) imaging. Imaging was performed on a Philips XL 40 Environmental SEM at 15 kV and a working distance of 10 mm. Backscatter images were taken of each wire cross-section along with a thin-window energy dispersive X-ray spectrographic (EDS) image of a representative cross-section.

Cross-sectional area (CSA) reduction and penetration rate calculations were performed in ImageJ software using backscatter images. Briefly, the nominal cross-sectional area for each section was first estimated using the circle or ellipse tool. Then, the actual cross-sectional area was measured using threshold adjustment and the magic wand tool. Using the CSA reduction values, the penetration rate of the wire at each month of implantation was calculated using Eq. (1), as presented in detail earlier [46].

$$p' = \frac{\left(\frac{A0}{\pi}\right)^{\frac{1}{2}} - \left(\frac{A(t)}{\pi}\right)^{\frac{1}{2}}}{t} \qquad (1)$$

2.3 Fourier transform infrared spectroscopy (FT-IR)

FT-IR was conducted in diffuse reflectance mode with a Jasco FTIR-4200 spectrophotometer. A series of 64 scans were performed at 4 cm^{-1} resolutions from 800 to 1600 cm^{-1}.

2.4 Histological processing and imaging

The portion of the extracted wire samples intended for histological analysis were snap-frozen in liquid nitrogen and cryo-sectioned [18]. Before staining, samples were preserved in a –80°C freezer. Cross sections were ethanol fixed and then stained with hematoxylin and eosin (H&E), mounted in Permount solution and imaged using an Olympus BX51, DP70 bright-field microscope. The granulation tissue was inspected around the implants.

2.5 Statistical analysis

All quoted errors and error bars correspond to the sample standard error.

3 Results

3.1 Metallographic analysis

Zinc wire cross-sections were observed to undergo progressive degradation while implanted *in vivo* in the rat artery wall (Figure 1). There was a steady decrease in the area of metallic zinc (bright area) over the course of implantation, with a noticeable difference in remaining metallic zinc between the 1 month and 20 month samples. Corrosion appeared to primarily occur at localized corrosion sites on the surface of the wires. Early corrosion began as localized pitting of the surface, which expanded and aggregated at later time points to cause comprehensive reduction in the cross-sectional area of the wire by 20 months.

Degraded metallic zinc was replaced by corrosion product (gray area) as time progressed. A majority of this corrosion product formed within the nominal cross-sectional area of the wire, and caused the implant to retain its original shape. Some corrosion product did infiltrate the surrounding tissue in later time points however, which was particularly evident in the 11 month and later time point images. Energy dispersive spectroscopy of the corrosion product found a large presence of O, Ca, and P, along with some remaining Zn (Figure 2). Oxygen (green) was generally found to be concentrated within the nominal cross-sectional area of the wire. This same area was also where trace Zn (yellow) was detected outside the remaining portion of non-corroded wire. Ca (magenta) and P (cyan) on the other hand were found to be predominantly located outside the nominal cross-sectional area and formed a layer encapsulating the zinc wire. This layer was also found to be responsible for the infiltration of corrosion product in the surrounding tissue. The quantity of O, Ca, and P present appears to increase and build up as corrosion progresses.

A similar yet more detailed inspection was conducted for the 12 month (Figure 3) and 20 month (Figure 4) specimens. After residing in the rat artery for 12 months, cross sections of Zn wires showed the presence of the following major elements: Zn, Ca, P, O, and C. The innermost layer consists mainly of Zn and O, followed by the distributions of Ca and P in almost identical regions. A C-containing layer was detected adjacent to the inner layer containing Zn, O, Ca and P, but not present at surfaces relatively lacking in corrosion activity. The even distribution of C at the outermost region was assumed to relate with the epoxy resin rather than from corrosion activity. Approximately 1/5 of the metallic area had corroded at 12 months. After 20 months, apart from the detection of the same major elements, about 1/2 of metallic area had corroded and the layers of all corrosion products were assumed much thicker and more evenly distributed.

The average CSA reduction values for the implanted Zn wires were observed to follow a linear correlation between area reduction and implantation time (Figure 5A). The amount of metallic Zn remaining for each wire decreased as the wire remained *in vivo* longer, with upwards of 55–60% cross-sectional area reduction for the 20 month sample. This linear correlation stayed true even at later time points.

Penetration rate values also loosely followed a linear correlation (Figure 5B), and the average penetration rate remained nearly constant at ~25 ± 10 μm/yr, with a significant variation, as implantation time increased for the Zn implant. As with cross-sectional area

reduction, this linear trend for penetration rate remained true at later time points as well. This steady corrosion penetration rate after an extensive period of implantation was highly unexpected in view of our results for 1 to 6 months reported earlier [38].

Scatter of the results is at least partially attributed to the *in vivo* model used in this study and associated effects on implant location and implant surface quality. Although the wire model allows for a low cost and simplified investigation at the interface between the metal and the host environment relative to the more costly, complex, and time consuming stent manufacturing and testing in larger animals (pigs, rabbits), the non-uniform fracturing of the brittle zinc oxide film covering the Zn implant is difficult to avoid during the wire implantation process. As discussed earlier [47], small or more extensive unavoidable bending of the wire affects the quality of the film in the bent sections, providing sites for uncontrolled and non-uniform corrosion that contributes to scatter in experimental data.

3.2 FT-IR analysis

FT-IR (infrared spectroscopy) spectra were used to examine the surface products present on explanted Zn wires after residing in the rat artery for 12 and 20 months (Figure 6). Since the cross sections of Zn wire were mounted in epoxy resin, which also absorbs FT-IR signals, the spectrum of the epoxy was first collected as a blank control. In the FT-IR spectrum of Zn wire cross sections, the PO_4^{3-} bands were present at 936 cm^{-1}, 943 cm^{-1} and 1134 cm^{-1}, which relates to the symmetrical stretching of the $\nu 1$ group (920–1000 cm^{-1}) [48] and asymmetric stretching of the $\nu 3$ group (1050–1180 cm^{-1}) [49,50], respectively. The CO_3^{2-} bands from the $\nu 2$ substitution were detected at 845 cm^{-1}, and CO_3^{2-} bands from the $\nu 3$ apatitic substitution were detected at 1395 cm^{-1}, 1431 cm^{-1}, and 1565 cm^{-1} [51,52]. Absorption intensities of PO_4^{3-} groups and CO_3^{2-} groups were higher at 20 months' residence compared to 12-month ones, indicating more production of those phases and improvement of phase properties making this phase more stable. This conforms well to the observation of thicker corrosion products from X-ray maps of Zn wires at longer residence (Figures 3 & 4).

3.3 Pourbaix diagrams

The production of the corrosion products in this system was also analyzed using the Pourbaix diagram (Figure 7 - calculated using FactSage 7.0 software). All of the thermodynamic equilibrium equations of Zn with the physiological ions present in H_2O are shown. Zn-H_2O and Zn-X-H_2O diagrams are shown for X = {C, P} and [Zn^{2+}]={10^{-6}}. The concentrations for HPO_4^{2-} and HCO_3^{-}(CO_2(aq)) in this diagram were set to be identical to the values in human blood plasma (0.001 mol/L for HPO_4^{2-}, and 0.027 mol/L for CO_2(aq)) [53]. The orange circles marked on the Pourbaix diagrams represent physiological conditions of tissue fluid (pH ≈ 7.4 and E ≈ 0.78 V) [40,60].

In the Zn-H_2O system, at low potentials of E < −1.0 V, Zn is in the immunity region and thus stable in the solid form. At surface potential E > −0.8 V, Zn^{2+} is stable at low pH while the ZnO phase forms at pH>8.3. At pH ≈ 7.4, the Zn-C-H_2O system reaches equilibrium with Zn^{2+} and $ZnCO_3$. As for the diagram of Zn-P-H_2O at physiological potential, both ZnP_2 and Zn_3P_2 dissolve, leaving ZnO the only solid product. No $Zn_3(PO_4)_2 \cdot 2H_2O$ was detected

under all conditions, indicating the presence of PO_4^{3-} FT-IR peaks may be due to the deposition of calcium phosphate.

Based on the signature of X-ray maps, the presence of PO_4^{3-} and CO_3^{2-} peaks from FT-IR, and the analysis of Pourbaix diagrams, it is speculated that after 12 month and 20 month in vivo, the layers of corrosion product surrounding the metallic Zn could be mixtures of ZnO, $ZnCO_3$ and calcium phosphate, as illustrated in the schematic phase maps (Figures 3 & 4). An electrochemical analysis of Zn wires corroded in vitro supports this interpretation (Supplemental Section). The present findings are consistent with our earlier analyses [38,40]. Longer residence of Zn wires in vivo was also qualitatively proven to lead to more production of corrosion products, which are more evenly distributed around the metallic wire.

3.4 Histological analysis

The inflammatory response elicited by the long-term presence of the Zn implant was characterized. A fibrotic and collagenous encapsulation response is evident in Figure 8. A progressively thickening collagenous capsule is shown in panels A-B. Panel F shows the thickest, most mature capsule of all time points.

Figure 8 shows the natural response of a living organism to "wall off" a foreign body. However, this process (as shown in panels C and D) is interrupted by spontaneous corrosion events along the wire. These corrosion events seem to continue through 20 months, as a thick, dense capsule develops to contain them. High cell density is present at 5, 6 and 8 months, which is indicative of chronic inflammation, possibly in relation to the steady corrosion activity. However, the chronic inflammation subsides between 10 and 20 months. There was no overt evidence of large scale cell toxicity detected at any time point.

4 Discussion

Zn wires implanted in the murine artery exhibited a steady and linear rate of biocorrosion. Specifically, it was observed that both CSA reduction and penetration rate were dependent on the time of implantation, a correlation that did not change significantly at later time points. This was supported both qualitatively (Figure 1), in which Zn wire cross-sections exhibited a continuous decrease in metallic area as the wires remained *in vivo* longer, and quantitatively (Figure 5), in which average values for both CSA reduction and penetration rate at each time point followed a linear correlation with implantation time.

It was also demonstrated that this linear corrosion progressed despite the formation of a passivating corrosion product layer around the wire. Energy dispersive X-ray spectroscopy revealed high levels of oxygen, calcium, and phosphorous around corroded implants (Figure 2). Together with FT-IR analysis of corrosion product and analysis of stable phases of an aqueous electrochemical system, it is concluded, in agreement with previous studies [38], that the major components of the corrosion product are zinc oxide (ZnO), zinc carbonate ($ZnCO_3$), and a calcium/phosphorous buffer layer. It was additionally hypothesized that the formation of a ZnO layer and enhanced mass transport would cause a gradual acceleration in the rate of implant corrosion [38]. However, this was not the case in the present study. The

formation of a thick oxide layer by 20 months of corrosion appeared to have no significant effect on the rate of implant degradation. The penetration rate did decrease long-term which might suggest some protective property of either the oxide or calcium/phosphorous buffer layers or both, but this ultimately had minimal effect on the overall reduction in cross-sectional area. This could be due in part to the lack of uniformity of the product layer. Previous studies on aqueous corrosion of Zn have identified that a two-layer porous patina forms on the surface capable of "self-repair" [54]. This process could be disrupted by cell and tissue growth around the implant, which could compromise the protective quality of the product layer. Another possibility is variations in local pH. Previous studies have shown the Zn corrosion rate to be controlled by the kinetics of cathodic reactions, either hydrogen evolution in acidic environments, or zinc hydroxide complex or zinc oxide formation in alkaline environments [55]. These formations can act to protect the Zn surface. However, a pH range of 7 – 10 is also associated with an ineffective corrosion protection barrier. Factors such as the rate of release of Zn^{2+} ions and formation of a buffer layer could maintain the local implant environment at a similar pH, compromising the integrity of the product layer, and maintaining the rate of corrosion.

Histological analysis indicated that fibrotic collagenous encapsulation of the wire implants initiated as early as 1 month post implantation (Figure 8). Encapsulation progressed as implantation time increased, with tissue growth a response to corrosion of the wire and chronic inflammation in the surrounding tissue. As with the corrosion product, however, the introduction of this capsule did not seem to have a significant impact on the degradation of the wire implants, even with a capsule upwards of a couple hundred microns thick at 20 months implantation. This could be due to the capsule achieving stability and containing what appear to be healthy cells, indicative of cell viability close to the degrading implant. Cellular Zn transport is a phenomenon observed in mammalian cells, including endothelial cells [56,57]. The presence of healthy cells around a Zn implant would potentially allow for continued transport of Zn^{2+} into surrounding capillaries, interstitial fluid, and blood and for degradation to continue at a constant rate, even with the emergence of a "physical" extracellular matrix barrier.

Encapsulation of the wire does seem to have a major effect on penetration rate over time, although the penetration rate is always well above zero. The change in penetration rate coincided with a reduction over time in the chronic inflammation intensity. Potentially the formation of a stable cellularized capsule contributed to a steady state environment, whereby continued bursts of zinc corrosion events along the implant were contained by the fibrous matrix (reducing both inflammation and penetration rate) and cleared by the resident cells (preventing cell toxicity). This balance highlights the effectiveness of the fibrous capsule in containing the corrosion events and thereby limiting the inflammatory response, yet still allowing cell mediated ionic transport and product clearance to take place. Further study will need to be done on the exact mechanism of Zn corrosion and interactions following formation of the cellular capsule.

Our findings of a cellularized capsule surrounding the zinc implant along with persistent biocorrosion activity at very late time points are very encouraging. Using the same *in vivo* wire implant model, we also found a cellularized capsule around zinc-aluminum alloys [45],

suggesting that both zinc and its alloys may become well integrated into surrounding biological tissue. We have recently reported that zinc luminal implants may suppress smooth muscle cell neointimal hyperplasia and promote the formation of a stable encapsulating neointimal tissue [42]. When taken together, the results suggest that a deployed zinc stent may suppress negative neointimal responses, promote the formation of a stable neointima lacking smooth muscle cells, and safely persist in biodegradation activity through functional breakdown of the implant.

Ultimately the observations made in this study support Zn as a candidate stent material and suggest Zn implants may meet general guidelines for a bioabsorbable stent [19]. An ideal bioabsorbable stent would retain mechanical integrity for 3–6 months. The implanted wires appear promising after exhibiting only around 15% CSA reduction after 6 months. Additionally, the Zn implants were observed to have penetration rates around the 20 μm/yr benchmark. The presence of viable cells around the wire at 20 months supports the recently reported biocompatibility of Zn [42,43]. The guidelines also state that full absorption of the implant should occur after 12–24 months [19], and the implants in this study showed only 60% CSA reduction at 20 months. It should be kept in mind however, that the diameter of implant wires was 0.25 mm, which is two-three times larger than the expected diameter of a stent strut. It suggests that the metallic Zn stent could corrode to corrosion products in less than 2 years, and could therefore comply with benchmark criteria.

Importantly, this study does reveal a linear model for the rate of Zn degradation *in vivo*, which would allow for simple prediction of implanted Zn behavior. This in turn could be used in the design of future biodegradable metallic implants to make them undergo full breakdown within the desired timetable.

When compared to studies of other degradable candidate stent metals in terms of long-term corrosion, Zn does not appear to suffer the same limitations. Despite showing signs of promising biocompatibility, *in vivo* corrosion of Fe stents for up to 18 months in the rabbit aorta revealed mild inflammation and discoloration of surrounding tissue [21], as well as a degradation rate that was lower than ideal. A similar conclusion was reached for the 12-month corrosion of Fe stents in the porcine aorta [17]. Studies with Mg faced the opposite challenge. Implantation of a Mg alloy in the medullary cavity of rabbits for up to 12 months produced up to 58% volume reduction by week 36 and 85% by week 52, despite an implant size of up to 2.5 mm diameter [58]. The implants were also associated with problematic biocompatibility, including loss of bone density. Another study employing subcutaneous implantation in rats saw up to 52% volume reduction by week 52 when PCL or PTMC-coated [59]. Comparatively, the Zn implants in the present study degraded at a rate between that of Fe and Mg for up to 20 months. 5

Conclusion

Corrosion of ϕ0.25 mm Zn wires implanted in murine artery for up to 20 months was characterized. Degradation of implants was found to progress linearly for both cross-sectional area reduction and penetration rate, with up to 60% CSA reduction at 20 months. Long-term implantation produced a thick corrosion layer and fibrotic encapsulation of the implants. Such formations contributed beneficially to implant bio-integration by suppressing

inflammation over the long term in a manner that did not prevent progressive corrosion. Ultimately, the observed rate of corrosion and biocompatibility of the implants support Zn as a candidate stent material. The proposed linear model makes it possible to predict *in vivo* implant behavior for the purposes of stent design. Further study is still needed to clarify the mechanism of interaction between the corroding implant, formed product, and the surrounding cellular layer.

Supplementary Material

Refer to Web version on PubMed Central for supplementary material.

Acknowledgments

References

1. Fischman DL, Leon MB, Baim DS, Schatz RA, Savage MP, Penn I, Detre K, Veltri L, Ricci D, Nobuyoshi M. A randomized comparison of coronary-stent placement and balloon angioplasty in the treatment of coronary artery disease. N. Engl. J. Med. 1994; 331:496–501. [PubMed: 8041414]

2. Serruys PW, de Jaegere P, Kiemeneij F, Macaya C, Rutsch W, Heyndrickx G, Emanuelsson H, Marco J, Legrand V, Materne P, Belardi J, Sigwart U, Colombo A, Goy JJ, van den Heuvel P, Delcan J, Morel M. A Comparison of Balloon-Expandable-Stent Implantation with Balloon Angioplasty in Patients with Coronary Artery Disease. N. Engl. J. Med. 1994; 331:489–495. [PubMed: 8041413]

3. Mani G, Feldman MD, Patel D, Agrawal CM. Coronary stents: A materials perspective. Biomaterials. 2007; 28:1689–1710. [PubMed: 17188349]

4. Farb A, Weber DK, Kolodgie FD, Burke AP, Virmani R. Morphological predictors of restenosis after coronary stenting in humans. Circulation. 2002; 105:2974–2980. [PubMed: 12081990]

5. Cook S, Wenaweser P, Togni M, Billinger M, Morger C, Seiler C, Vogel R, Hess O, Meier B, Windecker S. Incomplete stent apposition and very late stent thrombosis after drug-eluting stent implantation. Circulation. 2007; 115:2426–2434. [PubMed: 17485593]

6. Chung WS, Park CS, Seung KB, Kim PJ, Lee JM, Koo BK, Jang YS, Yang JY, Yoon JH, Kim D Il, Yoon YW, Park JS, Cho YH, Park SJ. The incidence and clinical impact of stent strut fractures developed after drug-eluting stent implantation. Int. J. Cardiol. 2008; 125:325–331. [PubMed: 17434616]

7. Onuma Y, Ormiston J, Serruys PW. Bioresorbable scaffold technologies. Circ. J. 2011; 75:509–20. [PubMed: 21301138]

8. Ormiston JA, Serruys PWS. Bioabsorbable coronary stents. Circ. Cardiovasc. Interv. 2009; 2:255–260. [PubMed: 20031723]

9. Tamai H, Igaki K, Tsuji T, Kyo E, Kosuga K, Kawashima A, Matsui S, Komori H, Motohara S, Uehata H, Takeuchi E. A Biodegradable Poly-l-lactic Acid Coronary Stent in the Porcine Coronary Artery. J. Interv. Cardiol. 1999; 12:443–450.

10. Bünger CM, Grabow N, Sternberg K, Goosmann M, Schmitz K-P, Kreutzer HJ, Ince H, Kische S, Nienaber CA, Martin DP. A biodegradable stent based on poly (Llactide) and poly (4-hydroxybutyrate) for peripheral vascular application: preliminary experience in the pig. J. Endovasc. Ther. 2007; 14:725–733. [PubMed: 17924740]

11. Grabow N, Bünger CM, Schultze C, Schmohl K, Martin DP, Williams SF, Sternberg K, Schmitz K-P. A biodegradable slotted tube stent based on poly (L-lactide) and poly (4-hydroxybutyrate) for rapid balloon-expansion. Ann. Biomed. Eng. 2007; 35:2031–2038. [PubMed: 17846893]

12. Tamai H, Igaki K, Kyo E, Kosuga K, Kawashima A, Matsui S, Komori H, Tsuji T, Motohara S, Uehata H. Initial and 6-month results of biodegradable poly-l-lactic acid coronary stents in humans. Circulation. 2000; 102:399–404. [PubMed: 10908211]

13. Heublein B, Rohde R, Kaese V, Niemeyer M, Hartung W, Haverich A. Biocorrosion of magnesium alloys: a new principle in cardiovascular implant technology? Heart. 2003; 89:651–656. [PubMed: 12748224]

14. Witte F, Hort N, Vogt C, Cohen S, Kainer KU, Willumeit R, Feyerabend F. Degradable biomaterials based on magnesium corrosion. Curr. Opin. Solid State Mater. Sci. 2008; 12:63–72.

15. Hermawan H, Alamdari H, Mantovani D, Dubé D. Iron–manganese: new class of metallic degradable biomaterials prepared by powder metallurgy. Powder Metall. 2008; 51:38–45.

16. Hermawan H, Purnama A, Dube D, Couet J, Mantovani D. Fe-Mn alloys for metallic biodegradable stents: Degradation and cell viability studies. Acta Biomater. 2010; 6:1852–1860. [PubMed: 19941977]

17. Peuster M, Hesse C, Schloo T, Fink C, Beerbaum P, von Schnakenburg C. Long-term biocompatibility of a corrodible peripheral iron stent in the porcine descending aorta. Biomaterials. 2006; 27:4955–4962. [PubMed: 16765434]

18. Pierson D, Edick J, Tauscher A, Pokorney E, Bowen P, Gelbaugh J, Stinson J, Getty H, Lee CH, Drelich J. A simplified in vivo approach for evaluating the bioabsorbable behavior of candidate stent materials. J. Biomed. Mater. Res. Part B Appl. Biomater. 2012; 100:58–67. [PubMed: 21905215]

19. Bowen PK, Shearier ER, Zhao S, Guillory RJ, Zhao F, Goldman J, Drelich JW. Biodegradable Metals for Cardiovascular Stents: from Clinical Concerns to Recent Zn•Alloys. Adv. Healthc. Mater. 2016; 5:1121–1140. [PubMed: 27094868]

20. Liu B, Zheng YF. Effects of alloying elements (Mn, Co, Al, W, Sn, B, C and S) on biodegradability and in vitro biocompatibility of pure iron. Acta Biomater. 2010; 252:151–156.

21. Peuster M, Wohlsein P, Brügmann M, Ehlerding M, Seidler K, Fink C, Brauer H, Fischer A, Hausdorf G. A novel approach to temporary stenting: degradable cardiovascular stents produced from corrodible metal—results 6–18 months after implantation into New Zealand white rabbits. Heart. 2001; 86:563–569. [PubMed: 11602554]

22. Lin W, Qin L, Qi H, Zhang D, Zhang G, Gao R, Qiu H, Xia Y, Cao P, Wang X. Long-term in vivo corrosion behavior, biocompatibility and bioresorption mechanism of a bioresorbable nitrided iron scaffold. Acta Biomater. 2017

23. Witte F, Fischer J, Nellesen J, Vogt C, Vogt J, Donath T, Beckmann F. In vivo corrosion and corrosion protection of magnesium alloy LAE442. Acta Biomater. 2010; 6:1792–1799. [PubMed: 19822226]

24. Witte F, Ulrich H, Rudert M, Willbold E. Biodegradable magnesium scaffolds: Part I: Appropriate inflammatory response. J. Biomed. Mater. Res. - Part A. 2007; 81:748–756.

25. Zhang Y, Xu J, Ruan YC, Yu MK, O'Laughlin M, Wise H, Chen D, Tian L, Shi D, Wang J, Chen S, Feng JQ, Chow DHK, Xie X, Zheng L, Huang L, Huang S, Leung K, Lu N, Zhao L, Li H, Zhao D, Guo X, Chan K, Witte F, Chan HC, Zheng Y, Qin L. Implant-derived magnesium induces local neuronal production of CGRP to improve bone-fracture healing in rats. Nat. Med. 2016

26. Gu XN, Zhou WR, Zheng YF, Cheng Y, Wei SC, Zhong SP, Xi TF, Chen LJ. Corrosion fatigue behaviors of two biomedical Mg alloys - AZ91D and WE43 - In simulated body fluid. Acta Biomater. 2010; 6:4605–4613. [PubMed: 20656074]

27. Kannan MB, Raman RKS. In vitro degradation and mechanical integrity of calcium-containing magnesium alloys in modified-simulated body fluid. Biomaterials. 2008; 29:2306–2314. [PubMed: 18313746]

28. Choudhary L, Raman RKS. Magnesium alloys as body implants: fracture mechanism under dynamic and static loadings in a physiological environment. Acta Biomater. 2012; 8:916–923. [PubMed: 22075121]

29. Song G. Control of biodegradation of biocompatable magnesium alloys. Corros. Sci. 2007; 49:1696–1701.

30. Razavi M, Fathi M, Savabi O, Razavi SM, Heidari F, Manshaei M, Vashaee D, Tayebi L. In vivo study of nanostructured diopside (CaMgSi2O6) coating on magnesium alloy as biodegradable orthopedic implants. Appl. Surf. Sci. 2014; 313:60–66.

31. Li Y, Wen C, Mushahary D, Sravanthi R, Harishankar N, Pande G, Hodgson P. Mg-Zr-Sr alloys as biodegradable implant materials. Acta Biomater. 2012; 8:3177–3188. [PubMed: 22531570]

32. Ding Y, Lin J, Wen C, Zhang D, Li Y. Mechanical properties, in vitro corrosion and biocompatibility of newly developed biodegradable Mg-Zr-Sr-Ho alloys for biomedical applications. Sci. Rep. 2016; 6

33. Zberg B, Uggowitzer PJ, Löffler JF. MgZnCa glasses without clinically observable hydrogen evolution for biodegradable implants. Nat. Mater. 2009; 8:887–891. [PubMed: 19783982]

34. Haude M, Erbel R, Erne P, Verheye S, Degen H, Böse D, Vermeersch P, Wijnbergen I, Weissman N, Prati F. Safety and performance of the drug-eluting absorbable metal scaffold (DREAMS) in patients with de-novo coronary lesions: 12 month results of the prospective, multicentre, first-in-man BIOSOLVE-I trial. Lancet. 2013; 381:836–844. [PubMed: 23332165]

35. Haude M, Ince H, Abizaid A, Toelg R, Lemos PA, von Birgelen C, Christiansen EH, Wijns W, Neumann F-J, Kaiser C. Safety and performance of the second-generation drug-eluting absorbable metal scaffold in patients with de-novo coronary artery lesions (BIOSOLVE-II): 6 month results of a prospective, multicentre, non-randomised, first-in-man trial. Lancet. 2016; 387:31–39. [PubMed: 26470647]

36. Haude M, Ince H, Abizaid A, Toelg R, Lemos PA, von Birgelen C, Christiansen EH, Wijns W, Neumann F-J, Kaiser C. Sustained safety and performance of the second-generation drug-eluting absorbable metal scaffold in patients with de novo coronary lesions: 12-month clinical results and angiographic findings of the BIOSOLVE-II first-in-man trial. Eur. Heart J. 2016:ehw196.

37. Alexy RD, Levi DS. Materials and manufacturing technologies available for production of a pediatric bioabsorbable stent. Biomed Res. Int. 2013; 2013

38. Bowen PK, Drelich J, Goldman J. Zinc exhibits ideal physiological corrosion behavior for bioabsorbable stents. Adv. Mater. 2013; 25:2577–2582. [PubMed: 23495090]

39. Zhao S, McNamara CT, Bowen PK, Verhun N, Braykovich JP, Goldman J, Drelich JW. Structural Characteristics and In Vitro Biodegradation of a Novel Zn-Li Alloy Prepared by Induction Melting and Hot Rolling. Metall. Mater. Trans. A. (n.d.). :1–12.

40. Zhao S, Seitz J-M, Eifler R, Maier HJ, Guillory RJ, Earley EJ, Drelich A, Goldman J, Drelich JW. Zn-Li alloy after extrusion and drawing: Structural, mechanical characterization, and biodegradation in abdominal aorta of rat. Mater. Sci. Eng. C. 2017; 76:301–312.

41. Bowen PK, Seitz J, Guillory RJ, Braykovich JP, Zhao S, Goldman J, Drelich JW. Evaluation of wrought Zn–Al alloys (1, 3, and 5 wt% Al) through mechanical and in vivo testing for stent applications. J. Biomed. Mater. Res. Part B Appl. Biomater. 2017

42. Bowen PK, Guillory RJ, Shearier ER, Seitz JM, Drelich J, Bocks M, Zhao F, Goldman J. Metallic zinc exhibits optimal biocompatibility for bioabsorbable endovascular stents. Mater. Sci. Eng. C. 2015; 56:467–472.

43. Shearier ER, Bowen PK, He W, Drelich A, Drelich J, Goldman J, Zhao F. In Vitro Cytotoxicity, Adhesion, and Proliferation of Human Vascular Cells Exposed to Zinc. ACS Biomater. Sci. Eng. 2016; 2

44. Fosmire GJ. Zinc toxicity. Am. J. Clin. Nutr. 1990; 51:225–227. [PubMed: 2407097]

45. Guillory RJ, Bowen PK, Hopkins SP, Shearier ER, Earley EJ, Gillette AA, Aghion E, Bocks M, Drelich JW, Goldman J. Corrosion characteristics dictate the long-term inflammatory profile of degradable zinc arterial implants. ACS Biomater. Sci. Eng. 2016; 2:2355–2364.

46. Bowen PKPK, Drelich A, Drelich J, Goldman J. Rates of in vivo (arterial) and in vitro biocorrosion for pure magnesium. J. Biomed. Mater. Res. - Part A. 2015; 103:341–349.

47. Drelich AJ, Bowen PK, LaLonde L, Goldman J, Drelich JW. Importance of oxide film in endovascular biodegradable zinc stents. Surf. Innov. 2016; 4:133–140.

48. Holt C, van Kemenade MJJM, Harries JE, Nelson LS, Bailey RT, Hukins DWL, Hasnain SS, De Bruyn PL. Preparation of amorphous calcium-magnesium phosphates at pH 7 and characterization by x-ray absorption and fourier transform infrared spectroscopy. J. Cryst. Growth. 1988; 92:239–252.

49. Bowen PK, Drelich J, Goldman J. Magnesium in the murine artery: Probing the products of corrosion. Acta Biomater. 2014; 10:1475–1483. [PubMed: 24296127]

50. Frost R, Martens W, Williams P, Kloprogge J. Raman and infrared spectroscopic study of the vivianite-group phosphates vivianite, baricite and bobierrite. Mineral. Mag. 2002; 66:1063–1073.

51. Gibson IR, Bonfield W. Preparation and characterization of magnesium/carbonate co-substituted hydroxyapatites. J. Mater. Sci. Mater. Med. 2002; 13:685–693. [PubMed: 15348578]

52. Meejoo S, Maneeprakorn W, Winotai P. Phase and thermal stability of nanocrystalline hydroxyapatite prepared via microwave heating. Thermochim. Acta. 2006; 447:115–120.

53. Kokubo T, Takadama H. How useful is SBF in predicting in vivo bone bioactivity? Biomaterials. 2006; 27:2907–2915. [PubMed: 16448693]

54. Thomas S, Birbilis N, Venkatraman MS, Cole IS. Self-repairing oxides to protect zinc: Review, discussion and prospects. Corros. Sci. 2013; 69:11–22.

55. Thomas S, Birbilis N, Venkatraman MS, Cole IS. Corrosion of zinc as a function of pH. Corros. J. Sci. Eng. 2012; 68:15001–15009.

56. Reyes JG. Zinc transport in mammalian cells. Am. J. Physiol. Physiol. 1996; 270:C401–C410.

57. Cousins RJ, Liuzzi JP, Lichten LA. Mammalian zinc transport, trafficking, and signals. J. Biol. Chem. 2006; 281:24085–24089. [PubMed: 16793761]

58. Dziuba D, Meyer-Lindenberg A, Seitz JM, Waizy H, Angrisani N, Reifenrath J. Long-term in vivo degradation behaviour and biocompatibility of the magnesium alloy ZEK100 for use as a biodegradable bone implant. Acta Biomater. 2013; 9:8548–8560. [PubMed: 22922249]

59. Wang J, He Y, Maitz MF, Collins B, Xiong K, Guo L, Yun Y, Wan G, Huang N. A surface-eroding poly(1,3-trimethylene carbonate) coating for fully biodegradable magnesium-based stent applications: Toward better biofunction, biodegradation and biocompatibility. Acta Biomater. 2013; 9:8678–8689. [PubMed: 23467041]

60. Cui, FZ., Feng, QL. Biomaterials Science (Chinese Edition). Tsinghua University Press; 2004.

Significance

Previous studies have shown zinc to be a promising candidate material for bioresorbable endovascular stenting applications. An outstanding question, however, is whether a zinc implant would ultimately passivate through the production of stable corrosion products or via a cell mediated tissue encapsulation process that prevented the diffusion of critical reactants and products at the metal surface. We found that zinc wires implanted in the murine artery exhibit steady corrosion for up to at least 20 months post-implantation. The results confirm earlier predictions that zinc stents could safely degrade within a time frame of approximately 1 – 2 years.
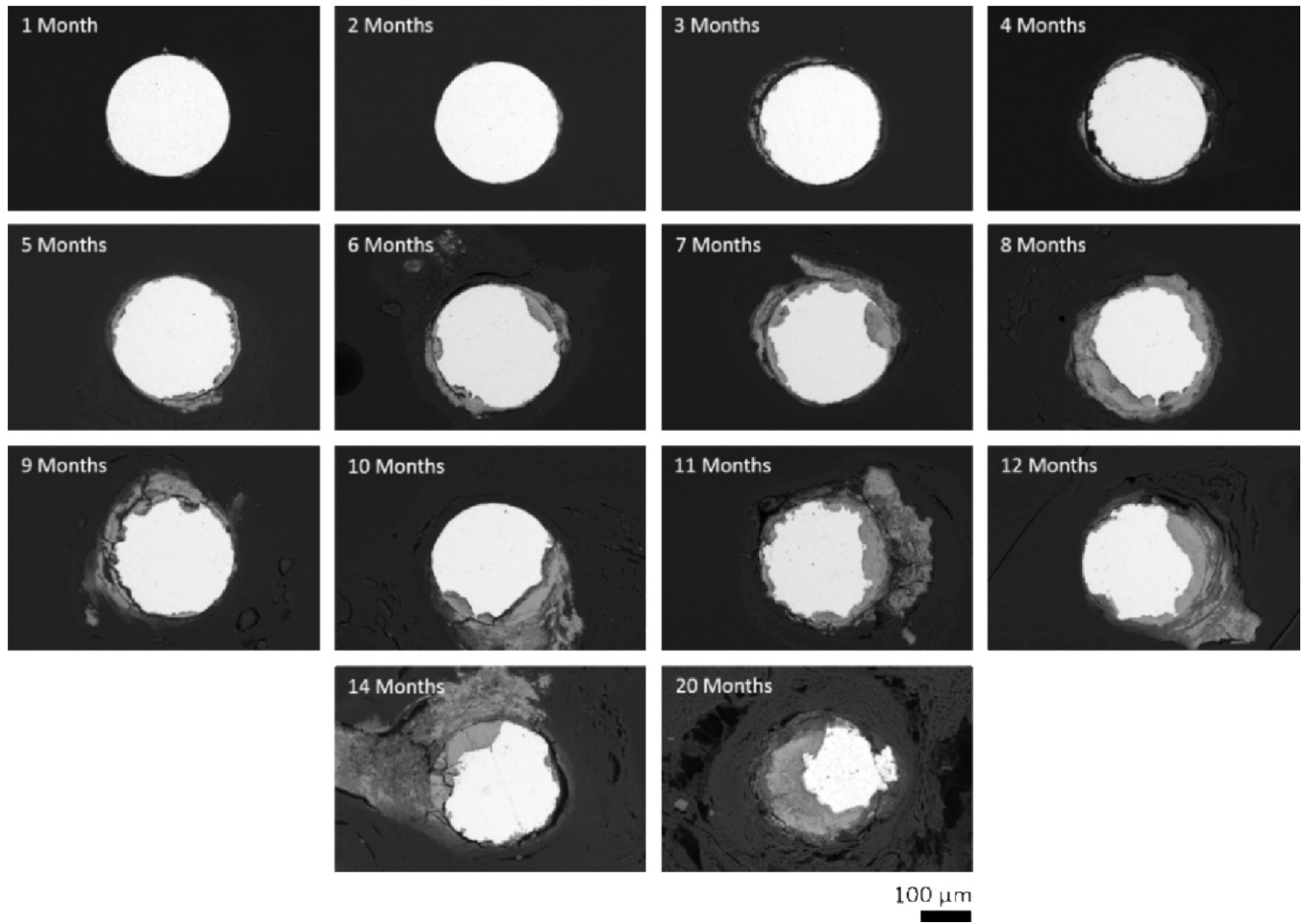
Figure 1.
Scanning electron backscatter images of representative zinc wire cross-sections.
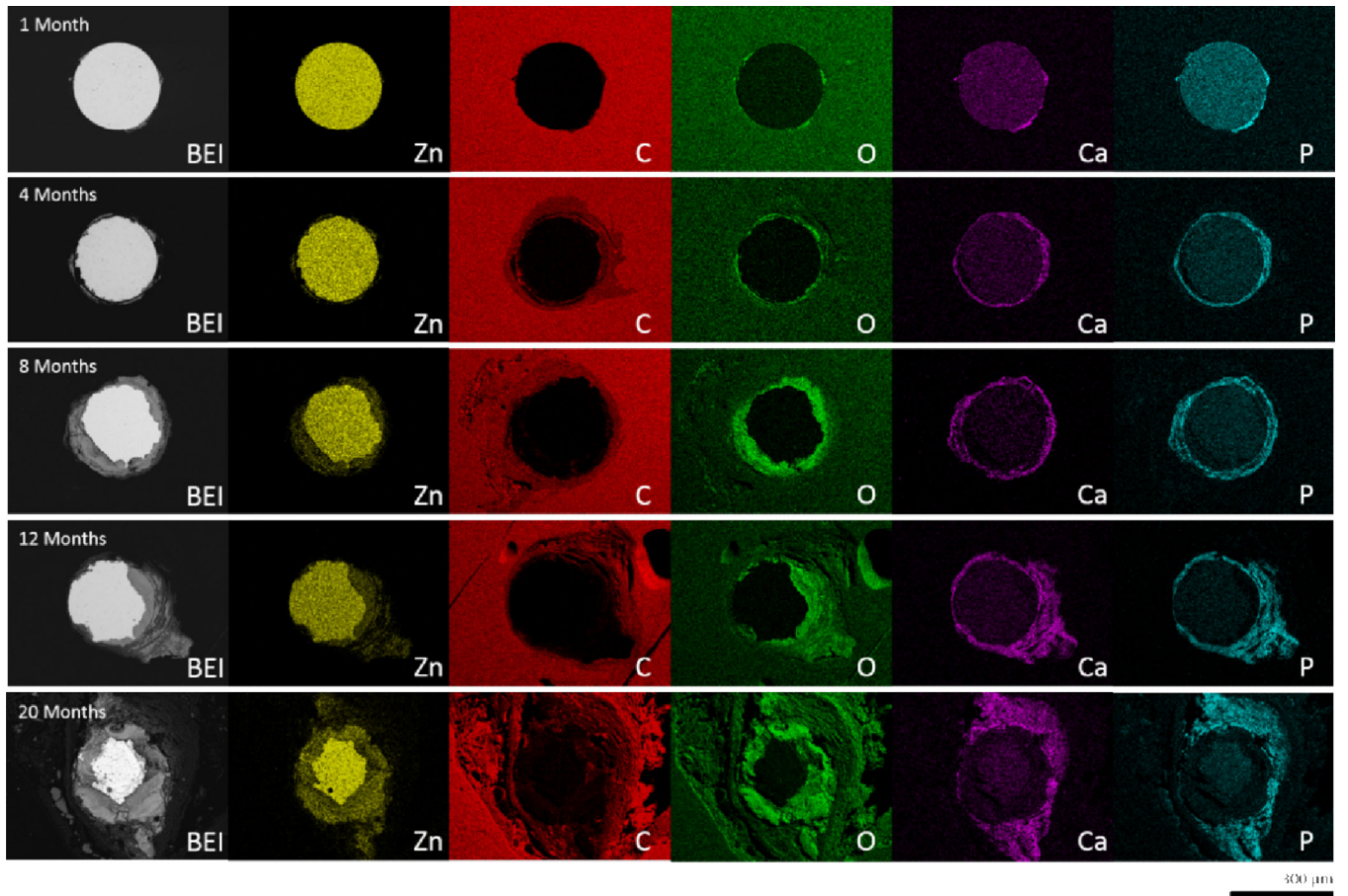
Figure 2.
Energy dispersive X-ray maps of representative zinc wire cross-sections.
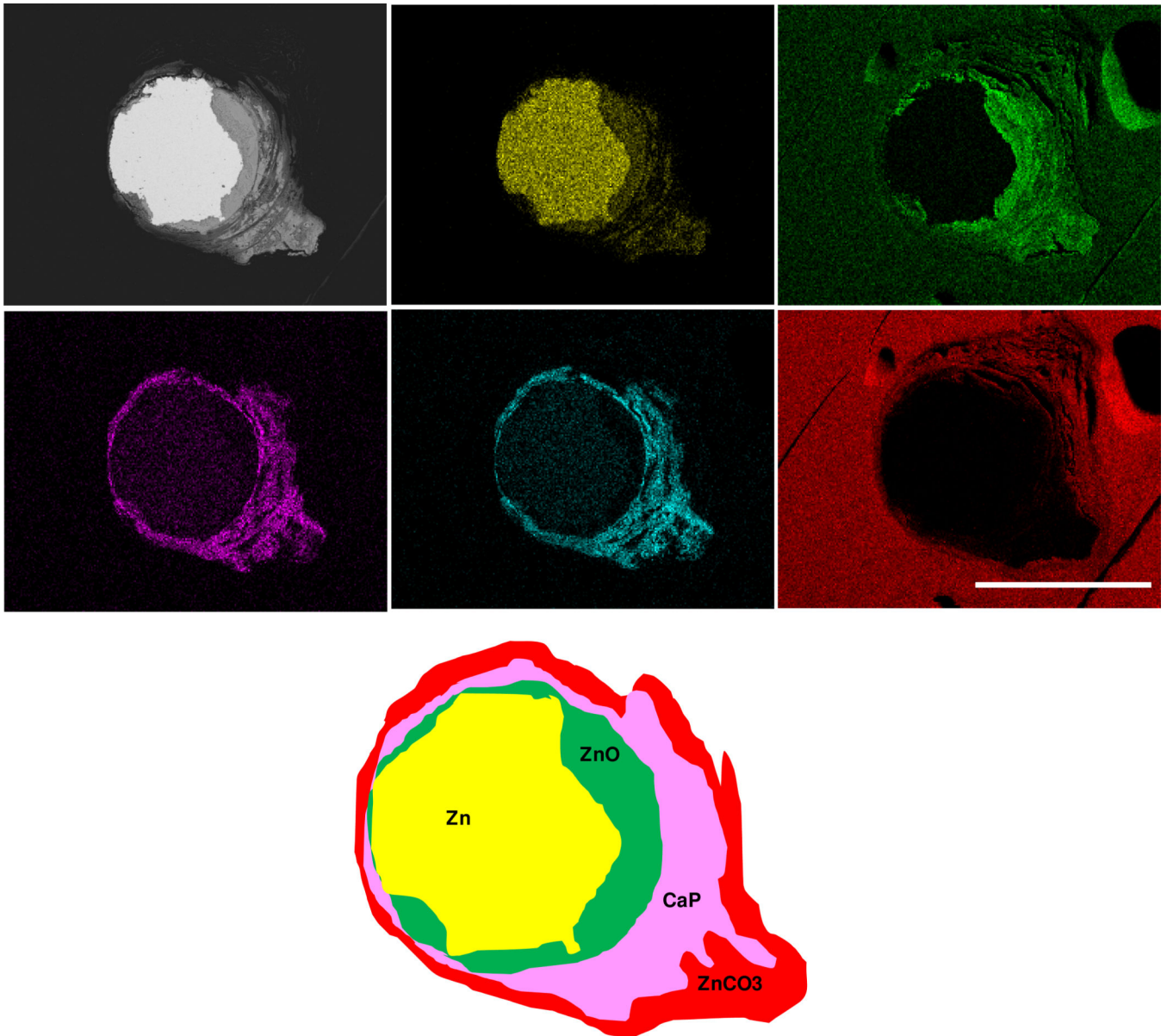
Figure 3.
Backscattered electron images and energy dispersive X-ray maps of Zn wire sections (enlarged view from Figure 2) and its schematic phase map after residing in the rat artery for 12 months.
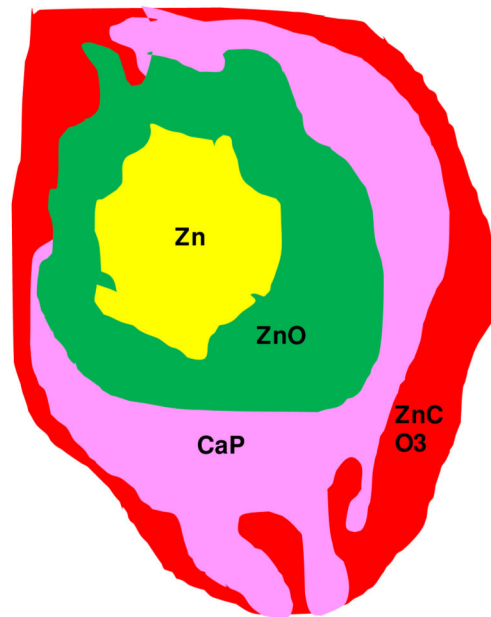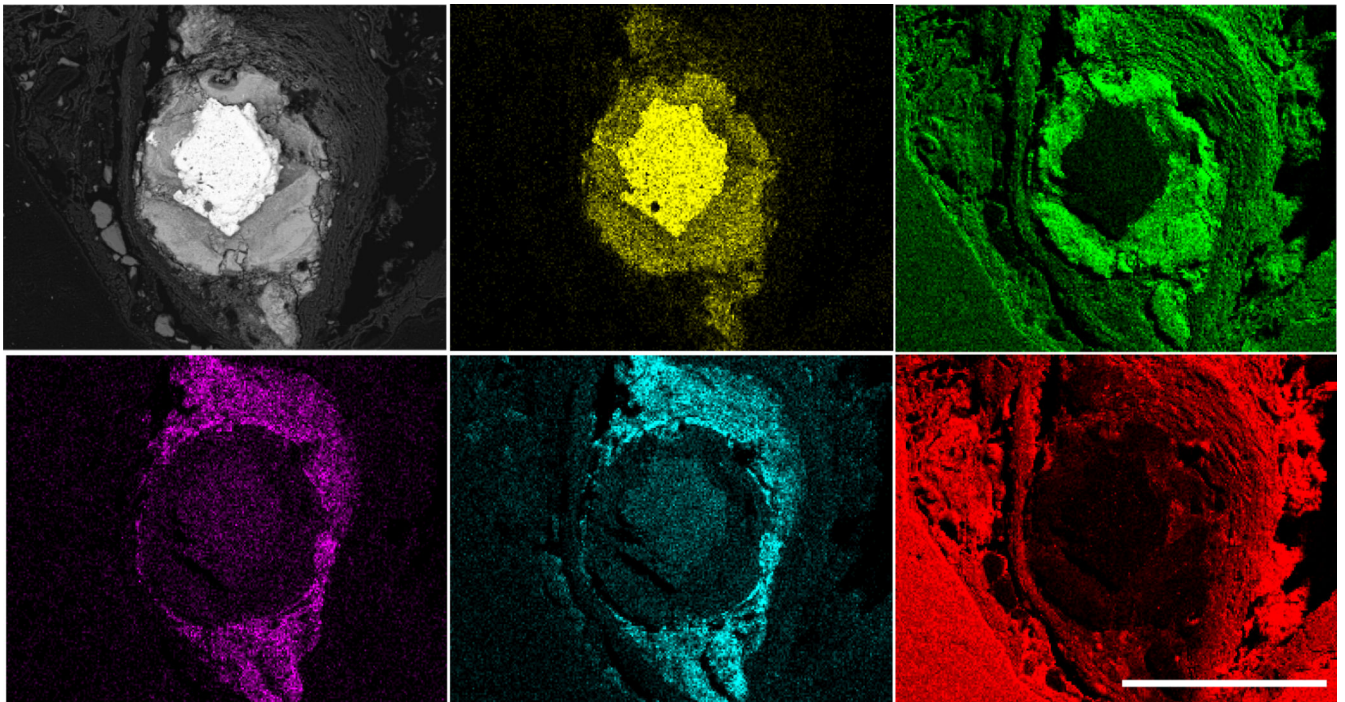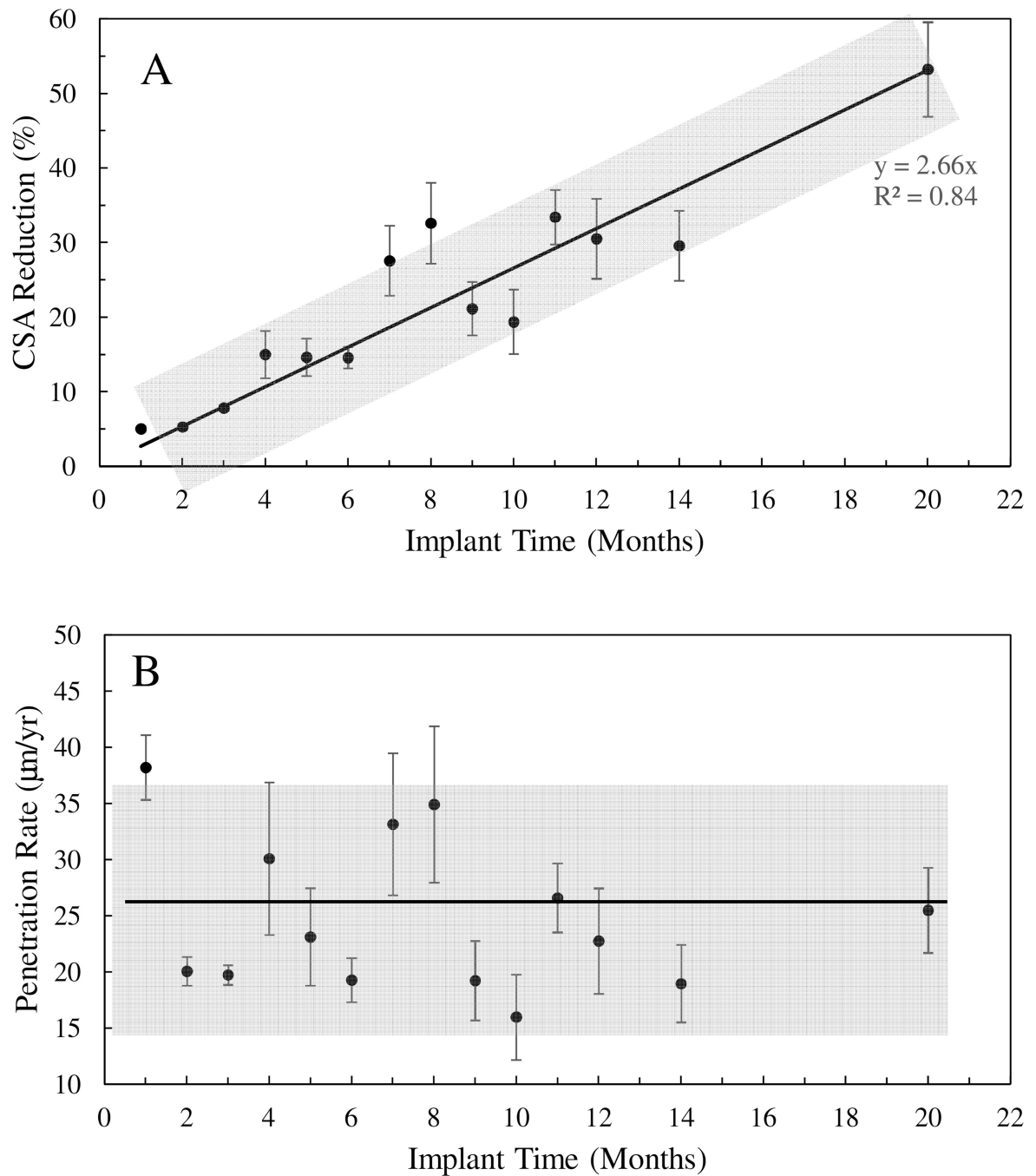
Figure 4.
Backscattered electron images and energy dispersive X-ray maps of Zn wire sections
(enlarged view from Figure 2) and its schematic phase map after residing in the rat artery for
20 months.

Figure 5.
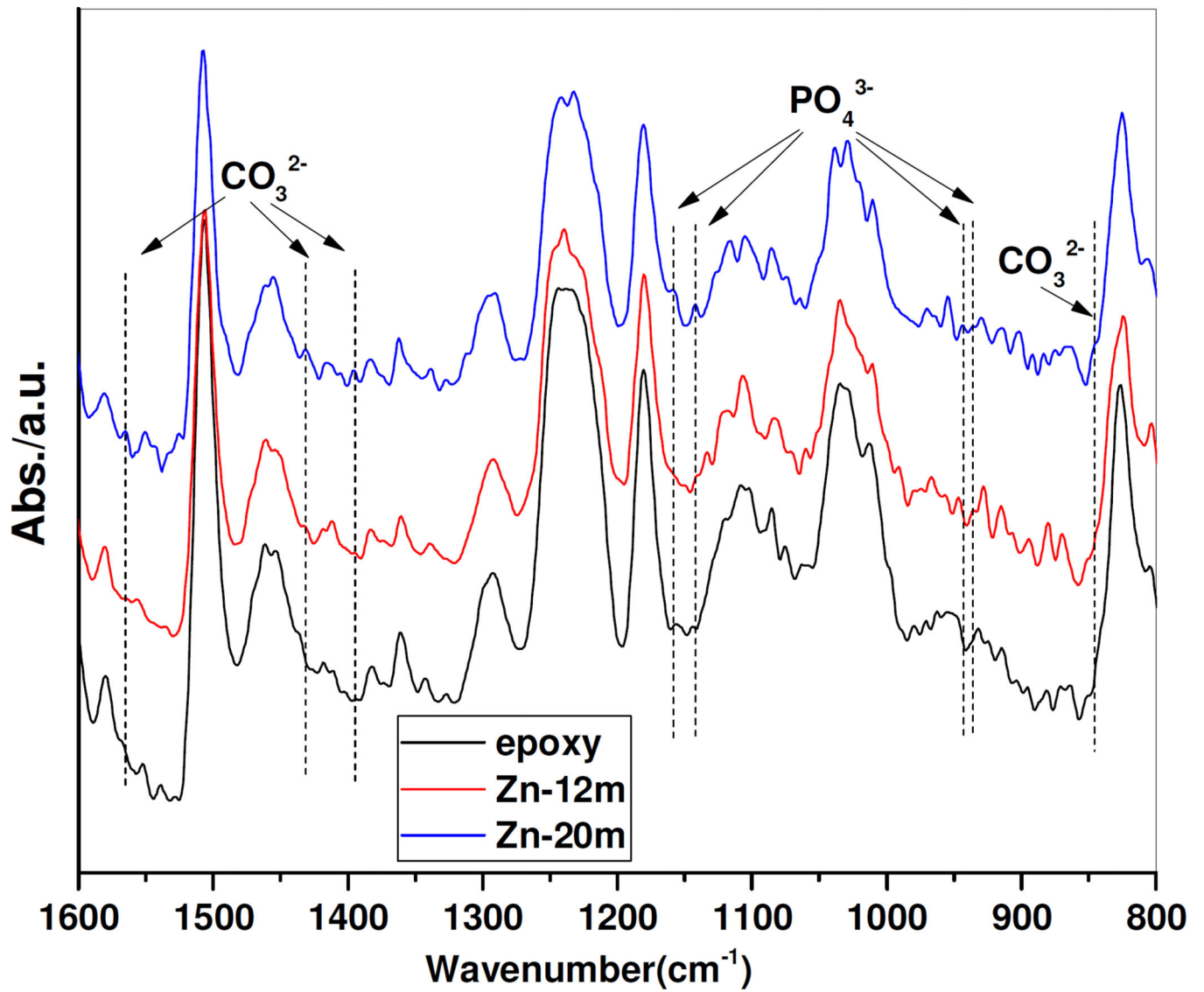Graphs of CSA reduction (A) and penetration rate (B) of implanted zinc wires as a function of implantation time.

Figure 6.
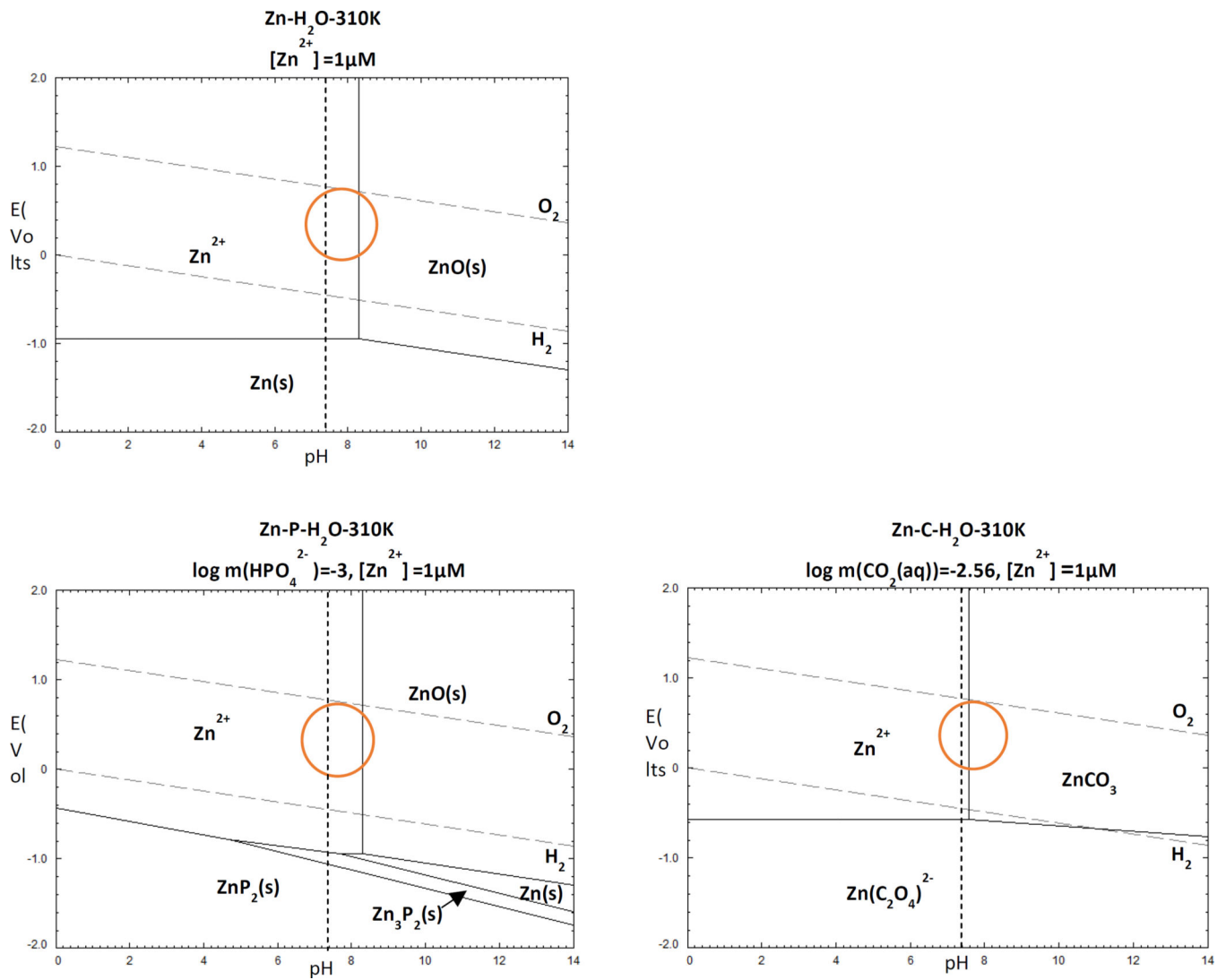FT-IR spectrum of Zn wire for 12-, and 20-month residence

Figure.7.
Zn-H$_2$O and Zn-H$_2$O-X Pourbaix diagrams for physiological concentrations of X = {C, P} at 37 °C. The dotted lines show physiological pH of 7.4. The physiological potential for tissue fluid is indicated by circles.
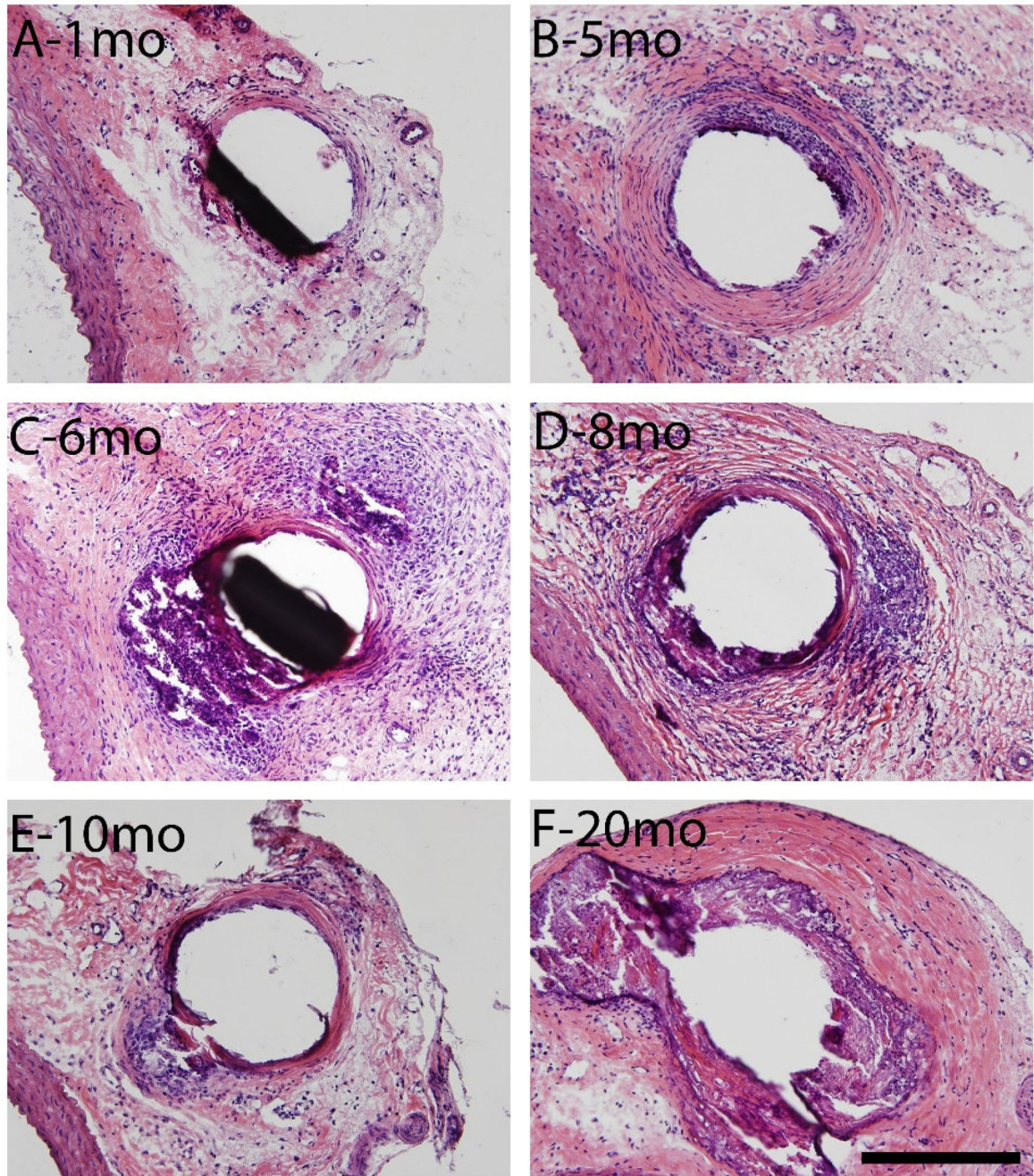
Figure 8.
Hematoxylin and eosin staining at 200X normal magnification of 1, 5, 6, 8, 10, and 20 month (A,B,C,D,E,F respectively) arterial wall implants of 4N zinc wires. Scale bar is 200 microns.